

# SPRNet: Single Pixel Reconstruction for One-stage Instance Segmentation

Jinghan Yao  
Hangzhou Dianzi University

Zhou Yu  
Hangzhou Dianzi University

Jun Yu  
Hangzhou Dianzi University

Dacheng Tao  
University of Sydney

## Abstract

Object instance segmentation is one of the most fundamental but challenging tasks in computer vision, and it requires the pixel-level image understanding. Most existing approaches address this problem by adding a mask prediction branch to a two-stage object detector with the Region Proposal Network (RPN). Although producing good segmentation results, the efficiency of these two-stage approaches is far from satisfactory, restricting their applicability in practice. In this paper, we propose a one-stage framework, SPRNet, which performs efficient instance segmentation by introducing a single pixel reconstruction (SPR) branch to off-the-shelf one-stage detectors. The added SPR branch reconstructs the pixel-level mask from every single pixel in the convolution feature map directly. Using the same ResNet-50 backbone, SPRNet achieves comparable mask AP to Mask R-CNN at a higher inference speed, and gains all-round improvements on box AP at every scale comparing to RetinaNet.

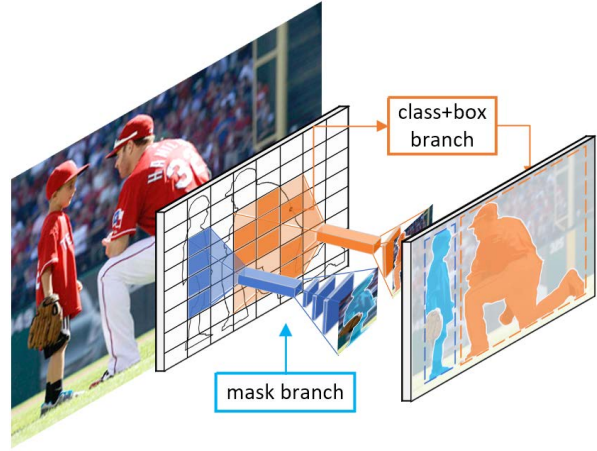


Figure 1: The SPRNet framework for instance segmentation. Classification, regression and mask branches are processed in parallel. We generate each instance mask from a single pixel, and resize it into its corresponding box to get the final instance-level prediction.

## 1 Introduction

Rapid developments in object detection and semantic segmentation have made it possible to accurately understanding region or pixel-level semantics. Combining object detection and semantic segmentation creates the more challenging instance segmentation task. Instance segmentation requires the correct class label prediction of all objects in an image while also precisely segmenting each instance. Optimally addressing this task would greatly benefit many applications including autonomous driving, robotics and video surveillance.

Most successful instance segmentation approaches are derived from object detection models, adding a new branch on top of regional features from Region Proposal Network (RPN) [22], to predict their corresponding masks [8, 12,

16]. In the well-known Mask R-CNN [8] framework, although the mask branch only adds a small computational overhead to its Faster R-CNN [22] backbone, its efficiency is still limited by its two-stage mechanism with a heavy head and multiple Regions of Interest (RoIs) [22].

Despite the success of two-stage detectors, in object detection task, current state-of-the-art one-stage detectors have reported similar accuracy and at faster speed. With carefully designed architectures [17, 21, 13] and loss functions [14], one-stage detectors are able to run in real-time. This gives rise to a natural question: *can we design a one-stage instance segmentation model that enjoys the dual benefits of efficiency and accuracy?*

The main problem in one-stage instance segmentation is how to distinguish instances between and within classes simultaneously from a convolution feature map without the help of pre-generated RoIs. To address this problem,

we propose a new framework, SPRNet (Figure 1). By using only a pixel to reconstruct the mask of an instance, our method compares to R-CNN based frameworks where the prediction of instance mask starts from each RoI, innovatively predicting the instance mask in a faster way and saving more memory, allowing more instances being predicted on an image. We use a group of convolutions with various dilations to gather enough information into a single pixel. To construct the mask of one instance, we sample a pixel and then use consecutive deconvolutions to construct a  $32 \times 32$  score map denoting the final mask prediction.

Since we have a strict requirement for information carried in a pixel, we also make modifications to the backbone part in our model. We borrow the principle from Feature Pyramid Network (FPN) [13], where features from different levels are added to construct a bottom-up and top-down path. In their implementation, a naive element-wise summation is used to fuse multi-level features. One the one hand, however, despite well-extracted semantic information from higher levels is fused into lower ones, more severe spatial shift from higher levels could also damage already well preserved spatial information on lower ones. Hence, this operation may introduce unconstrained information flow, which remains improvements. On the other hand, since the derivative of '+' is always a constant, summation will cause gradient propagation between each level, implicitly weakening the effect of the fused features, because the initiative of designing FPN is to detect objects in different scales on different levels, which means that gradient from one level should not easily interfere another. Therefore, we propose an improved Gate-FPN (GFPN) by explicitly introducing a simple gating mechanism before feature fusion. This step improves the quality of feature fusion and smartly restrict gradient propagation between different levels, leading to better detection and segmentation.

To summarize, SPRNet extends the state-of-the-art one-stage detector RetinaNet by adding a parallel branch for predicting an object mask. Note that SPRNet is a general framework, so the backbone network can be replaced with other one-stage detectors without damaging the integrity and feasibility of instance mask generation. Our main contributions are as follows: 1) we propose one-stage instance segmentation without any crop operations. SPRNet achieves comparable performance in terms of mask AP to Mask R-CNN, while delivering a faster speed at the inference; 2) by introducing the Gate-FPN architecture, we bring all-round improvements on AP in detection and segmentation performance.

## 2 Related work

**Object Detection:** Prevalent object detection approaches can be categorized into two classes: the two-stage framework based on region proposals [6, 22], or the one-stage framework based on convolutional feature maps [20, 17, 14]. As pioneered in the R-CNN work [22], the first stage generated a set of candidate region proposals to recall as much objects as possible, and the second stage use a deep networks to classify the proposals. Furthermore, R-CNN successfully underpinned many follow-up improvements like Faster R-CNN [22] and R-FCN [4], which are the current leading frameworks for object detection. An inevitable procedure of the two-stage methods is the per-proposal prediction. When a large number of proposals are utilized, this became a speed bottleneck of these methods. In contrast, the one-stage methods do not introduce the region proposals thus obtained a significant improvement on speed. OverFeat [23] was one of the first modern one-stage object detector based on deep networks. SSD [17] and YOLO [20] are carefully designed for high speed at the expense of lower accuracy. Recently, DSSD [5] and RetinaNet [14] have renewed interest in one-stage methods, achieving impressive accuracy that rivals that of two-stage detectors, and also running at much higher speeds.

**Instance Segmentation:** Combining the object detection task with the semantic segmentation task results in a more challenging instance segmentation task. Instance segmentation requires a pixel-level prediction between and within classes [7]. DeepMask [19] and subsequent works first generate candidate segment proposals, and then classify them by Fast R-CNN [6]. As the segmentation stage is time-consuming, these methods are usually slow. Fully Convolutional Instance Segmentation (FCIS) [12] embedded the segment proposal stage into an object detection framework. However, FCIS produced systematic errors for overlapping instances and creates spurious edges, demonstrating that it is challenged by the inherent difficulties in segmenting instances. Mask R-CNN extends Faster R-CNN by adding a branch for predicting segmentation masks on each Region of Interest (RoI) [8]. All the above instance segmentation approaches are two-stage that require to generate region (or segment) proposals first, which limited their running speed. Different from the one-stage object detectors that only need to predict rectangular boxes for describing objects, generating promising instance-level segmentation masks is beyond the capability of existing one-stage detectors.

**Bottom-up and Top-down:** In both the detection and segmentation tasks, the problem of detecting small objects is an open problem. On the bottom layers of a deep networks, objects have rich spatial information but lacking of clear semantic; while on the top layers the situation turn around. To tackle this problem, Feature Pyramid Network

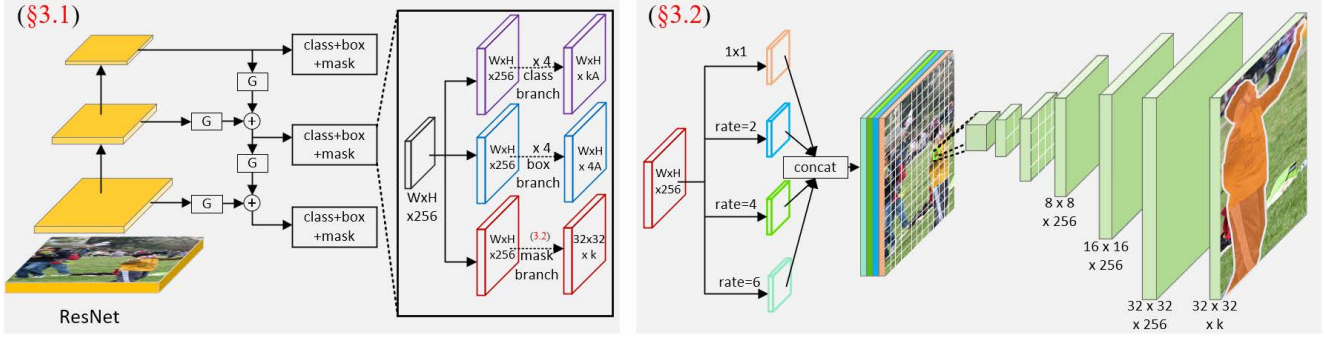


Figure 2: **SPRNet**: (3.1) Start with GPFN with ResNet-50 backbone, where  $G$  denotes the gate mechanism; then following three paralleled branches for predicting class, box and mask respectively. (3.2) Mask branch with multi-scale fusion, positive pixel sampling and consecutive deconvolutions for instance mask generation.

(FPN) was proposed to aggregate multi-level features in a pyramidal hierarchy. Beyond the traditional *bottom-up* pathway by the deep networks, (FPN) additionally established a *top-down* paths to deliver the rich semantic information of top layers to the bottom layers [13]. In their implementation, each top layer feature is  $2\times$  up-sampled and then merged with the bottom level feature using element-wise summation. By doing so, the semantic information of top layers can be passed to the bottom layers successfully. However, their inaccurate spatial information is also passed to the bottom layers at the same time, which *counteract* the effectiveness to some extent.

### 3 Single Pixel Reconstruction

To achieve the goal of one-stage instance segmentation, there are two core problems to be well resolved: 1) how to *encode* sufficient spatial and semantic information into each single pixel on the convolutional features; 2) how to *decode* the instance mask from feature with respect to a single pixel. In the following, we first introduce the network architecture of SPRNet, which is inspired by RetinaNet [14]. And motivated by the *deconvolution* introduced in the semantic segmentation models [1, 18], we propose a mask branch that consists of a cascade of deconvolution layers to reconstruct complete mask from a single pixel.

#### 3.1 Network Architecture

The network architecture of SPRNet is similar with RetinaNet [14], which is a one-stage object detector, with ResNet and FPN as its backbone. Our SPRNet introduce two modifications to make it better in detection and be able to deliver instance segmentation.

First, in FPN, higher features are up-sampled and directly added to lower ones. However, the reasoning be-

hind designing FPN is to achieve such a ‘bottom-up and top-down’ information flow between different levels, and common methods orientates each level to focus on a certain size range of objects. For example, a typical configuration is to set the anchor size to [32, 64, 128, 256, 512] at each level respectively. However, this relationship is not strictly proved. In ResNet [27, 9], each stage contains different number of layers, giving its final feature map different receptive fields, and their differences is of more probability to be rather than a naive  $2x$  relationship as how we set the anchor size. Therefore, simply adding features without any constraints may damage the integrity of some parts of the feature map.

Second, there is an issue implicitly in the naive adding operation. For example, the derivation of  $a$  in ‘ $a+b$ ’ is always equal to a constant, and the same for  $b$ . If we perform ‘+’ between two levels of features, then during gradient back-propagation [11], the loss from lower features will directly pass into higher ones. This violates the purpose of the pyramid structure, namely that different levels detect objects at different scales. In other words, we only want to use higher level’s features in lower ones but do not want the loss of lower ones to interfere with higher ones.

We call our solution Gated-FPN (GFPN). The purpose of GFPN is to enable the network to automatically determine which information needs to be passed into another level. The structure of GFPN is also illustrated in Figure 3, before adding, both features need to pass through a shared separable convolution layer, and then pass through a sigmoid activation to obtain each score map. The score map element-wise corresponds to each feature, with the value on score maps clearly being between zero and one. Then, we multiply two score maps with two features, respectively, after which we perform an adding operation. It can clearly be seen that before adding, some parts of each feature map will be close to zero while some parts will remain the same. Note that we share a separable convolution layer is naturally

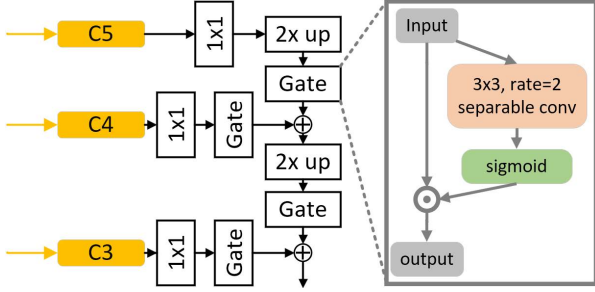


Figure 3: Gate mechanism in GFPN. Note that the separable convolution is shared by two features.

because we want to score each feature map under the same metric, while retaining better features and preventing worse ones, and we prefer separable convolution instead of normal convolution is simply because it reduces calculation and performs better.

To fairly evaluate the effectiveness of GFPN, we implement it on RetinaNet frameworks, and compare it with the original FPN. By introducing 0.05% more parameters, we improve box AP by up to 1.3, 2.3 and 4.3 points on small, medium and large objects on MS-COCO respectively. More details are shown in Table 2.

After GFPN, there following three branches — regression, classification and segmentation. Since the regression and classification branches are the same as those of RetinaNet, we ignore their details for simplicity. Note that three branches are processed in parallel, and they all based on GFPN, as shown in Figure 2. (3.1). At each GFPN level, we perform the same operations with shared parameters and they are used together to predict instances. During training, overall losses consist of three parts: classification, regression, and mask. We use the focal loss [14] as  $L_{cls}$ , the smoothed  $L_1$  loss [22] as  $L_{reg}$  and binary cross-entropy loss [8] as  $L_{mask}$ . Their exact forms are illustrated in [14, 22, 8] respectively.

### 3.2 Mask Branch

To achieve the goal of one-stage instance segmentation, two core problems need to be well resolved: 1) how to *encode* sufficient spatial and semantic information into each single pixel on the convolutional features; 2) how to *decode* the instance mask from features with respect to a single pixel. To address the two problems, we proposed an Encoder-and-Decoder-like structure. The encoder part we perform a multi-scale fusion so that details of object’s morphological information are embedded within each pixel. After that, we sample pixels which are most likely to locate at the center of any instances which are called positive pixels, and perform a decoder [2]-like reconstruction process. Each positive pixel is gradually reconstructed into a  $32 \times 32$  score map

which denotes the mask of its corresponding instance mask. See Figure 2. (3.2) for more details.

**Multi-scale Fusion:** To endow a single pixel with enough information, We use four different convolution operations before single pixels are sampled off, including a  $1 \times 1$  convolution with 256 channels and three  $3 \times 3$  convolutions with dilation rates at [2, 4, 6], and each has 128 channels. After concatenating these feature maps, each single pixel carries morphological information across various scales and has large receptive fields embedded. Note that the actual receptive field of consecutive convolutions and atrous convolutions is larger than the corresponding anchor size which is up to about 15, As noted above, we do it deliberately since the sampled pixel may not locate at the very center of an instance, it has to see ‘wider’ for better capturing information of the entire instance.

In order to select which pixels are possible to generate good mask, We first generate 9 anchor boxes on each pixel. If any one of its 9 boxes has an overlap larger than 0.7 (higher than the box training positive threshold of 0.5) with any instances, then we set this pixel to be a positive sample for training and its label is the instance’s mask that is resized to  $32 \times 32$  pixels. Note that pixels that are near the same instance have exactly the same training target, since they all locates on the same instance. More details are in Figure 6. We set the positive threshold to 0.7 because it is very clear that the higher the overlap threshold, the more probable it is that the sampled pixel is located close to the center of the instance, and vice versa. We need to leverage the best threshold for several reasons. First, a low threshold usually results in more sampled pixels being outside the instances, which makes it very hard to generate a preferable and accurate mask and makes training too difficult. In contrast, a high threshold makes the training relatively easy, but results in the network lacking robustness and stability. This is simply because during evaluation or inference, we sample pixels that correspond to the highest 100 classification scores, and we cannot guarantee that these pixels are at the very center of instances. Therefore, appropriately setting the overlap threshold becomes vital for training mask branch. In our ablation studies, we compare how different thresholds affect the final mAP. According to our results, a 0.7 threshold achieves robustness while retaining easy training.

**Single Pixel Reconstruction:** A shared decoder [2] is followed for each pixel, which starts from a  $1 \times 1$  pixel, using a series of operations to gradually reconstruct its segmentation mask. We first use three consecutive deconvolution layers with no activation to gradually generate its  $8 \times 8$  instance mask, after which we use the 2 times up-sample and then convolution method twice to construct the final mask. We also add a nearest interpolation shortcut from the  $8 \times 8$  mask to the final classification layer. Note



that at the first three deconvolutions, because each feature map is quite small, we do not use any activation, like *ReLU*. Although activation is widely used in normal convolutions, here it may set many neurons to zero, and destroy important information carried in the relatively small feature maps. As for the last two convolutions before the final classification layer, we use 2 times up-sample and then convolution operation. We stop using deconvolutions because, at this step, we need some spatial relationships between pixels so that better details and edges could be presented.

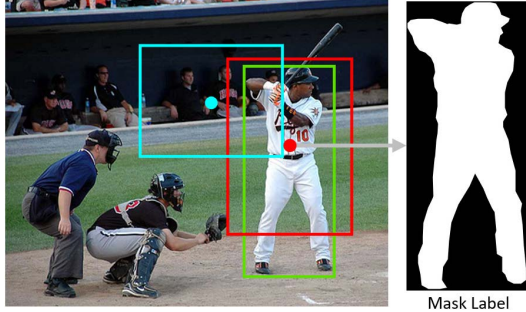


Figure 4: Green box is the target. Red box has an overlap greater than 0.7 with it, so the pixel at red dot is labeled as positive. Blue box is merely overlapped with the target, hence, blue dot is labeled as negative.

Also, another option is a  $3 \times 3$  deconvolution with stride=2, but the  $3 \times 3$  deconvolution kernel causes unexpected spatial overlaps and mosaicism which will result in poor segmentation, so we use two consecutive 2 times up-sample and then convolution to recover the instance mask to  $32 \times 32$  pixels, finally followed by a  $1 \times 1$  convolution for output. To get the final prediction, given a  $32 \times 32 \times 80$  mask map, we sample the highest channel according to the classification branch score to obtain the instance mask. In the loss part, we use binary cross-entropy function, and only calculate the on-class mask loss of all 80 classes.

### 3.3 Implementation details

Since one-stage instance segmentation is a brand new approach, important details will be thoroughly illustrated.

**Label Preparation:** In this part, we introduce how we prepare the training labels for mask prediction. As it is shown in Figure 5., according to anchors located at each pixel, the first step is to filter out anchors with an overlap larger than 0.7 with any target boxes, then sort them in descending order and train the network only on the highest 300 anchors. Since each anchor is located at one pixel, we use 300 pixels corresponding to the 300 anchors. Each pixel is responsible for generating its corresponding instance.

We use 3 different sizes and 3 different ratios to generate anchor boxes on every pixel, which generates 9 anchors in

total on every pixel at each level of the feature maps. In box labeling, we set anchors that overlap with any instance labels larger than 0.5 as positive anchors, and those less than 0.4 as negative ones. And in mask generation, we set the positive threshold to 0.7.

**Training:** SPRNet is easy to train. We train a total 25 epochs on the MS-COCO 2017 `train` dataset using Adam optimizer with initial learning rate of  $10^{-5}$  and gradient clip at  $10^{-3}$ . We use ResNet backbone that pre-trained on ImageNet, and train the entire network end-to-end. Other schedules may report slightly different results than those reported here.

**Inference:** During inference, the only difference is that we no longer use anchor overlap as the metric to sample pixels since there are no target labels, so we use pixels with the highest 100 scores outputted by the classification branch, and after each sampled pixel is reconstructed into a  $32 \times 32$  instance mask, we use bilinear interpolation to resize them to the actual box size outputted by the regression branch.

## 4 Experiments: Instance Segmentation

In this section, we provide comparative experiments to the current state-of-the-art methods, along with comprehensive ablation experiments. All the experiments are conducted on MS-COCO dataset [15]. We report the standard MS-COCO metrics including AP, AP<sub>50</sub>, AP<sub>75</sub> and AP<sub>S</sub>, AP<sub>M</sub> and AP<sub>L</sub> (AP at different scales). We report the results in terms of box AP and mask AP jointly. Follow the previous work in [8], we train using 115k train images (`train`), and report ablations on the 5k val images (`val`).

### 4.1 Main Results

We compare SPRNet to the state-of-the-art instance segmentation methods in Table 1. All instantiations of our model have comparable performance to previous state-of-the-art models including MNC [3], FCIS [12] and Mask R-CNN [8], the winners of MS-COCO 2015, 2016 and 2017 segmentation challenges, respectively. Without embellishments or any data augmentation, SPRNet with the ResNet-50-GFPN backbone has a lower 1.6 AP compared to Mask R-CNN with ResNet-50-FPN, which also includes horizontal flip training, and online hard example mining (OHEM) [24].

Due to the natural advantage of one-stage detectors, detection results have a higher recall than R-CNN based frameworks 3. Also, our method could robustly distinguish edges on overlapped objects. Note that the overlap issue is extremely severe in FCIS, and later solved by Mask R-CNN. Our one-stage SPRNet has shown good capability of

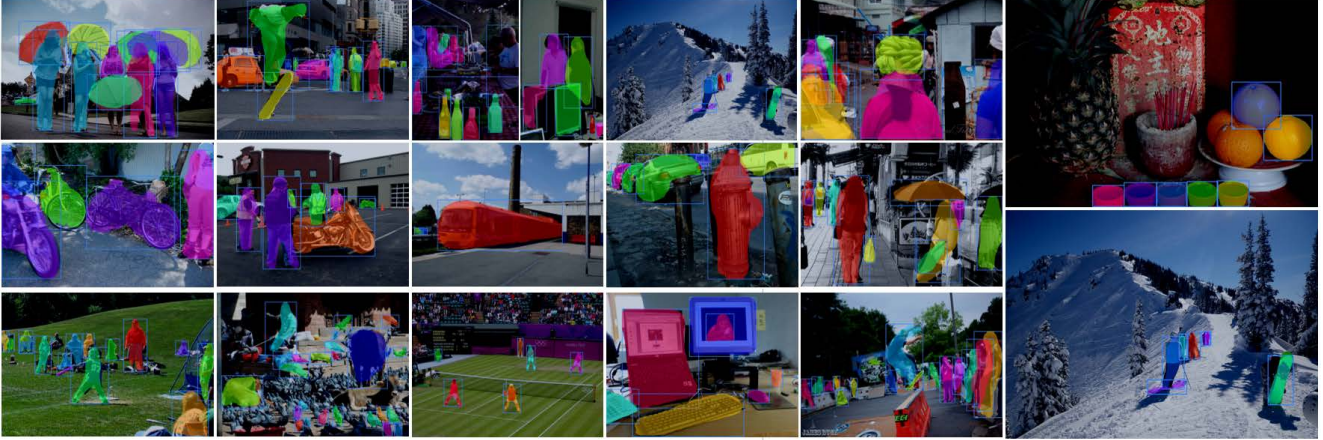


Figure 5: **Instance segmentation:** SPRNet generates boxes and masks with high accuracy and recall. Each instance is drawn in a distinguished color.

	fps	scale	backbone	AP	AP <sub>50</sub>	AP <sub>75</sub>	AP <sub>S</sub>	AP <sub>M</sub>	AP <sub>L</sub>
<b>Two-stage methods</b>									
MNC [3]	-	800	ResNet-101-C4	24.6	44.3	24.8	4.7	25.9	43.6
FCIS [12]+OHEM [24]	-	800	ResNet-101-C5-dilated	29.2	49.5	-	7.1	31.3	50.0
FCIS +++[12]+OHEM [24]	-	800	ResNet-101-C5-dilated	33.6	54.5	-	-	-	-
Mask R-CNN	7	800	ResNet-50-FPN	33.6	55.2	35.3	-	-	-
Mask R-CNN	-	800	ResNet-101-C4	33.1	54.9	34.8	12.1	35.6	51.1
Mask R-CNN	5	800	ResNet-101-FPN	35.7	<b>58.0</b>	37.8	15.5	38.1	52.4
Mask R-CNN	5	800	ResNet-101-GFPN	<b>36.0</b>	57.9	<b>38.0</b>	<b>16.0</b>	<b>38.5</b>	<b>54.0</b>
<b>One-stage methods</b>									
SPRNet (Ours)	<b>10</b>	500	ResNet-50-FPN	29.8	52.8	30.0	11.3	32.6	48.9
SPRNet (Ours)	<b>10</b>	500	ResNet-50-GFPN	30.4	53.2	30.8	12.4	33.3	49.6
SPRNet (Ours)	<b>9</b>	800	ResNet-50-GFPN	32.0	54.3	32.1	13.8	34.5	49.3
SPRNet	<b>7</b>	800	ResNet-101-GFPN	<b>34.0</b>	<b>56.6</b>	<b>34.4</b>	<b>14.9</b>	<b>35.4</b>	<b>50.6</b>

Table 1: We report mAP on MS-COCO 2017 val dataset, the result shows that our model is not as powerful as Mask R-CNN but runs at a higher speed. Since SPR Net is based on one-stage frameworks, it is natural to have these results.

handling this issue. We visualize some examples of the SPRNet predictions in Figure 5. SPRNet achieves good results even under challenging conditions.

## 4.2 Ablation Experiments

To better understand the reason of SPRNet’s effectiveness, we run a number of ablations. Results are shown in Table 5 and discussed in detail below.

**Fusion Paths:** In Table 1(a), we show two alternative strategies to obtain one pixel with large receptive fields. **C33x4:** four *consecutive*  $3 \times 3$  convolutions, which is as same as the classification or the regression branch; **C33-1,2,4,6:** four *parallel*  $3 \times 3$  convolutions with different dilation rates [1,2,4,6], which has similar computation costs to C33x4, but is able to capture more the morphological transformation of an instance. Results show a 1.2 point

AP improvement. Moreover, as increasing of object shapes, their performance gap gets larger.

**FPN vs. GFPN:** Table 1(b) ablates the performance gap between FPN and the proposed GFPN. We provide the comparative results under mask mAP and box mAP. When evaluating box predictions, we remove the mask branch from SPRNet thus making it degrade to a RetinaNet variant with GFPN. Results show GFPN outperforms FPN steadily under all criteria.

**Mask Generation with Shortcuts:** Table 1(c) compares the methods w/ or w/o shortcut connection. For the Deconv+shortcut model, we add an additional shortcut from  $8 \times 8$  feature map (with  $4 \times$  upsampling) to the final classification layer, and it improves the AP score by 0.4.

**Mask IoU Threshold:** Table 1(d) compares the models trained with different mask IoU threshold when preparing training samples. A small threshold (e.g., 0.5) results in



Figure 6: Mask R-CNN vs. SPRNet. With the natural advantage of one-stage frameworks, SPRNet has a higher recall than Mask R-CNN (the first column), while Mask R-CNN has better performance in instance details.

(a) Fusion Paths						
	AP	AP <sub>50</sub>	AP <sub>75</sub>	AP <sub>S</sub>	AP <sub>M</sub>	AP <sub>L</sub>
C33x4	29.2	52.1	30.0	12.2	32.4	48.6
C33-1,2,4,6	30.4	53.2	30.8	12.4	33.3	49.6

(b) FPN vs. GFPN						
	AP <sup>m</sup>	AP <sub>50</sub> <sup>m</sup>	AP <sub>75</sub> <sup>m</sup>	AP <sup>bb</sup>	AP <sub>50</sub> <sup>bb</sup>	AP <sub>75</sub> <sup>bb</sup>
FPN	29.8	52.8	30.0	32.5	50.9	34.8
GFPN	30.4	53.2	30.8	33.6	52.0	35.9

(c) Mask Generation with Shortcuts						
	AP	AP <sub>50</sub>	AP <sub>75</sub>	AP <sub>S</sub>	AP <sub>M</sub>	AP <sub>L</sub>
Deconv	30.0	52.9	30.5	12.4	32.6	49.2
Deconv+shortcut	30.4	53.2	30.8	12.4	33.3	49.6

(d) Mask IoU Threshold						
Overlap	AP	AP <sub>50</sub>	AP <sub>75</sub>	AP <sub>S</sub>	AP <sub>M</sub>	AP <sub>L</sub>
> 0.5	30.2	53.0	30.6	12.1	33.3	49.3
> 0.7	30.4	53.2	30.8	12.4	33.3	49.6

Table 2: Ablation experiments concern three main parts of SPRNet and mask valid threshold on final mAP. (a) **Fusion Paths**: Before pixels are sampled off, which way do we choose to fuse information into it. (b) **FPN vs. GFPN**: The improvement brought by gate mechanism. (c) **Mask Generation with Shortcuts**: Adding an shortcut in the final mask generation could bring a higher accuracy. (d) **Mask IoU Threshold**: A proper threshold could maximize the performance.

an inferior AP score. This could be explained that a small threshold makes it hard to converge for training.

### 4.3 Analysis

We compare SPRNet and Mask R-CNN in Figure 6, with each instance drawn in a distinguished color. Both two methods use the same ResNet-50 backbone. The samples include objects at various scales. Our method shows comparable performance to Mask R-CNN in most of the cases. Specifically, Mask R-CNN has a higher accuracy (i.e., more accurate mask boundaries for the detected objects) while SPRNet has a higher recall (i.e., more objects are detected). Mask R-CNN beats SPRNet in extreme situations with more detailed and aligned predictions. We recognize that there remains a gap between one- and two-stage frameworks for this task, which is natural because that during evaluation, Mask R-CNN uses its final box predictions to accurately sample RoIs, making mask prediction a very easy binary semantic segmentation task. In contrast, one-stage frameworks must find another totally different but plausible approach to generate instance masks. Despite using powerful atrous convolution to collect spatial

information into a single pixel, it is still challenging to recover a very detailed and accurate mask. Also, due to the limitation of the one-stage framework, regression values will largely influent the final accuracy in both box and mask AP. For regression boxes that are seriously shifted from the ground truths boxes, mask could easily be misaligned, which is the limitation of SPRNet. At the expanse of accuracy, SPRNet delivers a higher speed. SPRNet runs at a faster speed. Under the same experimental settings (i.e., GTX 1080Ti), Mask R-CNN using ResNet-50-FPN as the backbone runs at 7 fps, while our SPRNet runs at 9 fps, which is about 30% faster.

## 5 Additional Experiments

Along with mask Average Precision evaluation metric, we provide two more sets of experiments, concerning the AP of object detection and Average Recall of both object detection and instance segmentation. As mentioned above, SPRNet has two innovations, the GFPN is dedicated to both box and mask branches, we illustrate that on certain conditions where only box detection is required, SPRNet could also outperform RetinaNet, especially in some more



	backbone	$AR_1^{box}$	$AR_{10}^{box}$	$AR_{100}^{box}$	$AR_S^{box}$	$AR_M^{box}$	$AR_L^{box}$
Mask R-CNN	ResNet-101-FPN	32.0	50.1	52.4	32.3	56.7	67.5
Mask R-CNN	ResNet-101-GFPN	<b>32.9</b>	<b>51.2</b>	<b>53.5</b>	<b>32.8</b>	<b>57.5</b>	<b>69.0</b>
RetinaNet	ResNet-50-FPN	30.7	49.1	52.0	32.0	56.9	68.0
RetinaNet	ResNet-50-GFPN	31.6	50.0	53.1	34.4	57.6	68.6
RetinaNet	ResNet-101-FPN	32.2	50.8	53.8	34.1	58.4	70.5
RetinaNet	ResNet-101-GFPN	<b>33.1</b>	<b>51.8</b>	<b>54.9</b>	<b>36.6</b>	<b>59.2</b>	<b>71.0</b>

Table 3: (test on val) Box ARs of RetinaNet and Mask-RCNN with or without GFPN. Significant improvement on ARs can be observed.

	backbone	$AR_1^{seg}$	$AR_{10}^{seg}$	$AR_{100}^{seg}$	$AR_S^{seg}$	$AR_M^{seg}$	$AR_L^{seg}$
Mask R-CNN	ResNet-101-FPN	29.9	45.7	47.6	26.2	51.8	65.1
Mask R-CNN	ResNet-101-GFPN	<b>30.3</b>	<b>45.9</b>	<b>47.7</b>	<b>26.3</b>	<b>51.7</b>	<b>64.7</b>
SPRNet	ResNet-50-FPN	28.6	44.6	46.9	26.0	52.0	65.1
SPRNet	ResNet-50-GFPN	29.5	45.4	47.9	27.9	52.7	65.6
SPRNet	ResNet-101-FPN	30.0	46.1	48.5	27.7	53.4	67.5
SPRNet	ResNet-101-GFPN	<b>30.9</b>	<b>47.0</b>	<b>49.5</b>	<b>29.7</b>	<b>54.1</b>	<b>68.0</b>

Table 4: (test on val) Segmentation ARs of SPRNet and Mask-RCNN with or without GFPN. Significant improvement on ARs can be observed.

detailed categories. It’s noteworthy that as the input size increases, RetinaNet shows a downtrend in large objects detection, while SPRNet effectively alleviates this problem, and this is due to the GFPN which confines gradients from lower levels to interfere with higher ones, making the FPN like structure performs as similar as ordinary C4 or C5-based frameworks in large objects detection. We also compare AR results of RetinaNet, Mask R-CNN and SPRNet, experiments show that SPRNet has largely increased the overall quantity of small objects being detected, as well as medium and large ones.

## 5.1 Recall on objects

One of the most important metrics to evaluate the detection performance is the *Average Recall*. Given an image, the more instances are detected, the higher AR it will get.

For two-stage detectors, recalls could be considered in two parts. The first is FPN’s recall, where anchors will be classified as positive or negative, and only positive boxes will be sent into following subnetworks, where the final recall is derived. While in one-stage frameworks, without proposal network, we will only get one recall.

In Table 3 and Table 4, we compare Mask R-CNN, RetinaNet and SPRNet in both object detection and instance segmentation tasks.

Implemented on Mask R-CNN and RetinaNet, Gate-FPN has largely increased the AR under all metrics. By simply importing Gate-FPN, SPRNet has not only surpassed Mask R-CNN in overall AR, but also achieved

prominent improvements on small object detection. The results prove that Gate-FPN is a very solid and flexible module for general use in different detection frameworks.

## 5.2 BBox Detection

We compare SPRNet with the state-of-the-art MS-COCO bounding-box object detection in Table 5. With an input size of 500 pixels, we achieve 1.1 percents’ improvement in box AP compared with best one-stage detector RetinaNet.

To analyze the effect of the gating mechanism for FPN, we conduct experiments to compare RetinaNet with GFPN or traditional FPN and the results are demonstrated in Table ???. By introducing the gate mechanism, the RetinaNet with GFPN outperforms the other one with FPN by 1.2, 1.6 and 3.1 percents’ in AP for small, medium and large object detection, respectively. The effectiveness of gradient blocking is also shown in Table ??, with an improvement of up to 4.3 percents’ in AP for large object detection. Similarly, the effectiveness of the gating mechanism is well shown by the AP improvement of up to 1.8 percents’ for small object.

Using ResNet-50 as the backbone, SPRNet easily beats all existing one-stage methods. Our elaborately designed gating mechanism has shown promising effects in solving previously mentioned problems of the common ‘bottom up’ structure. By automatically abandoning inferior information between features, we find a promising approach to improve the performance of detecting small objects. By



	backbone	$AP^{bb}$	$AP_{50}^{bb}$	$AP_{75}^{bb}$	$AP_S^{bb}$	$AP_M^{bb}$	$AP_L^{bb}$
<b>1.2pt Two-stage methods</b>							
Faster R-CNN+++	ResNet-101-C4	34.9	55.7	37.4	15.6	38.7	50.9
Faster R-CNN w FPN	ResNet-101-FPN	36.2	59.1	39.0	18.2	39.0	48.2
Faster R-CNN by G-RMI [10]	Inception-ResNet-v2 [26]	34.7	55.5	36.7	13.5	38.1	52.0
Faster R-CNN w TDM [25]	Inception-ResNet-v2-TDM	36.8	57.7	39.2	16.2	39.8	52.1
Faster R-CNN, RoIAlign	ResNet-101-FPN	37.3	59.6	40.3	19.8	40.2	48.8
Mask R-CNN	ResNet-101-FPN	38.2	60.3	41.7	20.1	41.1	50.2
<b>0.8pt One-stage methods</b>							
YOLO v2 [21]	Darknet-19	21.6	44.0	19.2	5.0	22.4	35.5
YOLO v3 608x608	Darknet-53	33.0	57.9	34.4	18.3	35.4	41.9
DSSD513	ResNet-101-DSSD	33.2	53.3	35.2	13.0	35.4	<b>51.1</b>
RetinaNet 500	ResNet-50-FPN	32.5	50.9	34.8	13.9	35.8	46.7
RetinaNet 800	ResNet-50-FPN	35.7	55.0	38.5	18.9	38.9	46.3
SPRNet (Ours) 500	ResNet-50-GFPN	33.6	52.1	35.9	15.1	37.4	49.7
SPRNet (Ours) 800	ResNet-50-GFPN	<b>36.0</b>	<b>55.3</b>	<b>38.8</b>	<b>20.2</b>	<b>39.6</b>	48.6

Table 5: **Object Detection:** box AP on MS-COCO. The comparison between famous one and two-stage frameworks shows that using the same backbone, SPRNet with GFPN has surpassed every existing one-stage detectors with a remarkable improvement on small object detection accuracy.

scale	GFPN?	$AP^{bb}$	$AP_{50}^{bb}$	$AP_{75}^{bb}$	$AP_S^{bb}$	$AP_M^{bb}$	$AP_L^{bb}$
400	✓	30.5	<b>47.8</b>	32.7	11.2	33.8	46.1
		<b>31.1</b>	47.3	<b>32.9</b>	<b>11.5</b>	<b>34.9</b>	<b>50.4</b>
500	✓	32.5	50.9	34.8	13.9	35.8	46.7
		<b>33.6</b>	<b>52.0</b>	<b>35.9</b>	<b>15.0</b>	<b>37.4</b>	<b>49.8</b>
600	✓	34.3	53.2	36.9	16.2	37.4	47.4
		<b>35.0</b>	<b>54.0</b>	<b>37.5</b>	<b>17.8</b>	<b>39.0</b>	<b>49.9</b>
700	✓	35.1	54.2	37.7	18.0	39.3	46.4
		<b>35.6</b>	<b>54.7</b>	<b>38.0</b>	<b>18.6</b>	<b>39.8</b>	<b>48.9</b>
800	✓	35.7	55.0	38.5	18.9	38.9	46.3
		<b>36.0</b>	<b>55.2</b>	<b>38.8</b>	<b>20.1</b>	<b>39.6</b>	<b>48.6</b>

Table 6: **Object Detection:** box AP of RetinaNet with FPN or GFPN. We use ResNet-50 as the common backbone, and we compare detailed AP under different input sizes. We report box AP without training or using the mask branch, which means we directly compare FPN and GFPN in terms of detection.

blocking gradient flows, larger objects detection becomes isolated to smaller ones, which yields more than 2 percents’ improvement in final AP.

In Table ??, we compare only the effect of GFPN by removing the mask branch both in training and inference. It is noteworthy that the RetinaNet’s detection accuracy of large objects is far less than our methods. As we mentioned before, GFPN provides a better way to feature fusion, and this is the reason of improvements on small object detection. In the meanwhile, GFPN restricts the gradient propagation from low levels into higher levels, and this is the reason of improvements on large object detection. These improvements happen on every input scale. More importantly, on the metric of  $AP_{50}$ , GFPN has been improved by up to 1.1 percents in AP, which means

more objects are likely to be well detected. On the metric of  $AP_{75}$ , GFPN has outperformed FPN by up to 1.1 percents in AP, and this is very important for practical application because our methods delivers more accurate detection on objects that are most likely to be detected. We do not try other input scale that is smaller than 400 or larger than 800 pixels, the reason is that existing ResNet backbone may fail in extracting spatial information when objects get too small, and convolution kernels may also be limited in receptive fields when objects get too large.

## 6 Conclusions

We present the SPRNet as a one-stage approach to image instance segmentation, without introducing the region pro-

posals. SPRNet achieves comparable performance with the state-of-the-art two-stage models while running at a faster speed. By introducing GFPN, we bring one-stage detectors into a higher level in that we enable it to deliver better detection than prevalent one- and two-stage detectors. This work represents a feasible solution for delivering accurate and fast instance-level recognition.

## References

- [1] L.-C. Chen, G. Papandreou, I. Kokkinos, K. Murphy, and A. L. Yuille. Deeplab: Semantic image segmentation with deep convolutional nets, atrous convolution, and fully connected crfs. *IEEE transactions on pattern analysis and machine intelligence*, 40(4):834–848, 2018. [3](#)
- [2] L.-C. Chen, Y. Zhu, G. Papandreou, F. Schroff, and H. Adam. Encoder-decoder with atrous separable convolution for semantic image segmentation. *arXiv preprint arXiv:1802.02611*, 2018. [4](#)
- [3] J. Dai, K. He, and J. Sun. Instance-aware semantic segmentation via multi-task network cascades. In *Proceedings of the IEEE Conference on Computer Vision and Pattern Recognition*, pages 3150–3158, 2016. [5](#), [6](#)
- [4] K. J. Dai and Y. L. R-FCN. Object detection via region-based fully convolutional networks. arxiv preprint. *arXiv preprint arXiv:1605.06409*, 2016. [2](#)
- [5] C.-Y. Fu, W. Liu, A. Ranga, A. Tyagi, and A. C. Berg. Dssd: Deconvolutional single shot detector. *arXiv preprint arXiv:1701.06659*, 2017. [2](#)
- [6] R. Girshick. Fast r-cnn. In *Proceedings of the IEEE international conference on computer vision*, pages 1440–1448, 2015. [2](#)
- [7] B. Hariharan, P. Arbeláez, R. Girshick, and J. Malik. Simultaneous detection and segmentation. In *European Conference on Computer Vision*, pages 297–312. Springer, 2014. [2](#)
- [8] K. He, G. Gkioxari, P. Dollár, and R. Girshick. Mask r-cnn. In *Computer Vision (ICCV), 2017 IEEE International Conference on*, pages 2980–2988. IEEE, 2017. [1](#), [2](#), [4](#), [5](#)
- [9] K. He, X. Zhang, S. Ren, and J. Sun. Deep residual learning for image recognition. In *Proceedings of the IEEE conference on computer vision and pattern recognition*, pages 770–778, 2016. [3](#)
- [10] J. Huang, V. Rathod, C. Sun, M. Zhu, A. Korattikara, A. Fathi, I. Fischer, Z. Wojna, Y. Song, S. Guadarrama, et al. Speed/accuracy trade-offs for modern convolutional object detectors. In *IEEE CVPR*, volume 4, 2017. [9](#)
- [11] Y. LeCun, B. E. Boser, J. S. Denker, D. Henderson, R. E. Howard, W. E. Hubbard, and L. D. Jackel. Handwritten digit recognition with a back-propagation network. In *Advances in neural information processing systems*, pages 396–404, 1990. [3](#)
- [12] Y. Li, H. Qi, J. Dai, X. Ji, and Y. Wei. Fully convolutional instance-aware semantic segmentation. *arXiv preprint arXiv:1611.07709*, 2016. [1](#), [2](#), [5](#), [6](#)
- [13] T.-Y. Lin, P. Dollár, R. B. Girshick, K. He, B. Hariharan, and S. J. Belongie. Feature pyramid networks for object detection. In *CVPR*, volume 1, page 4, 2017. [1](#), [2](#), [3](#)
- [14] T.-Y. Lin, P. Goyal, R. Girshick, K. He, and P. Dollár. Focal loss for dense object detection. *IEEE transactions on pattern analysis and machine intelligence*, 2018. [1](#), [2](#), [3](#), [4](#)
- [15] T.-Y. Lin, M. Maire, S. Belongie, J. Hays, P. Perona, D. Ramanan, P. Dollár, and C. L. Zitnick. Microsoft coco: Common objects in context. In *European conference on computer vision*, pages 740–755. Springer, 2014. [5](#)
- [16] S. Liu, L. Qi, H. Qin, J. Shi, and J. Jia. Path aggregation network for instance segmentation. In *Proceedings of the IEEE Conference on Computer Vision and Pattern Recognition*, pages 8759–8768, 2018. [1](#)
- [17] W. Liu, D. Anguelov, D. Erhan, C. Szegedy, S. Reed, C.-Y. Fu, and A. C. Berg. Ssd: Single shot multibox detector. In *European conference on computer vision*, pages 21–37. Springer, 2016. [1](#), [2](#)
- [18] J. Long, E. Shelhamer, and T. Darrell. Fully convolutional networks for semantic segmentation. In *Proceedings of the IEEE conference on computer vision and pattern recognition*, pages 3431–3440, 2015. [3](#)
- [19] P. O. Pinheiro, R. Collobert, and P. Dollár. Learning to segment object candidates. In *Advances in Neural Information Processing Systems*, pages 1990–1998, 2015. [2](#)
- [20] J. Redmon, S. Divvala, R. Girshick, and A. Farhadi. You only look once: Unified, real-time object detection. In *Proceedings of the IEEE conference on computer vision and pattern recognition*, pages 779–788, 2016. [2](#)
- [21] J. Redmon and A. Farhadi. Yolo9000: better, faster, stronger. *arXiv preprint*, 2017. [1](#), [9](#)
- [22] S. Ren, K. He, R. Girshick, and J. Sun. Faster r-cnn: Towards real-time object detection with region proposal networks. In *Advances in neural information processing systems*, pages 91–99, 2015. [1](#), [2](#), [4](#)
- [23] P. Sermanet, D. Eigen, X. Zhang, M. Mathieu, R. Fergus, and Y. LeCun. Overfeat: Integrated recognition, localization and detection using convolutional networks. *arXiv preprint arXiv:1312.6229*, 2013. [2](#)
- [24] A. Shrivastava, A. Gupta, and R. Girshick. Training region-based object detectors with online hard example mining. In *Proceedings of the IEEE Conference on Computer Vision and Pattern Recognition*, pages 761–769, 2016. [5](#), [6](#)
- [25] A. Shrivastava, R. Sukthankar, J. Malik, and A. Gupta. Beyond skip connections: Top-down modulation for object detection. *arXiv preprint arXiv:1612.06851*, 2016. [9](#)
- [26] C. Szegedy, S. Ioffe, V. Vanhoucke, and A. A. Alemi. Inception-v4, inception-resnet and the impact of residual connections on learning. In *AAAI*, volume 4, page 12, 2017. [9](#)
- [27] S. Xie, R. Girshick, P. Dollár, Z. Tu, and K. He. Aggregated residual transformations for deep neural networks. In *Computer Vision and Pattern Recognition (CVPR), 2017 IEEE Conference on*, pages 5987–5995. IEEE, 2017. [3](#)